Computational fluid dynamic
modeling of a medium-sized surface mine blasthole drill shroud

by Y. Zheng, W.R.Reed, L. Zhou and J.P. Rider

Abstract ■ The Pittsburgh Mining Research Division of the U.S. National Institute for Occupational Safety and Health (NIOSH) recently developed a series of models using computational fluid dynamics (CFD) to study airflows and respirable dust distribution associated with a medium-sized surface blasthole drill shroud with a dry dust collector system. Previously run experiments conducted in NIOSH's full-scale drill shroud laboratory were used to validate the models. The setup values in the CFD models were calculated from experimental data obtained from the drill shroud laboratory and measurements of test material particle size. Subsequent simulation results were compared with the experimental data for several test scenarios, including 0.14 m^3/s (300 cfm) and 0.24 m^3/s (500 cfm) bailing airflow with 2:1, 3:1 and 4:1 dust collector-to-bailing airflow ratios. For the 2:1 and 3:1 ratios, the calculated dust concentrations from the CFD models were within the 95 percent confidence intervals of the experimental data. This paper describes the methodology used to develop the CFD models, to calculate the model input and to validate the models based on the experimental data. Problem regions were identified and revealed by the study. The simulation results could be used for future development of dust control methods for a surface mine blasthole drill shroud.

Y. Zheng, W.R. Reed and J.P. Rider, members SME, are associate service fellow, research mining engineer and acting team leader, respectively, Dust, Ventilation and Toxic Substances Branch (DVTSB), and L. Zhou, member SME, is associate service fellow, Fires and Explosions Branch (FEB), at the Pittsburgh Mining Research Division (PMRD), U.S. National Institute for Occupational Safety and Health (NIOSH), Pittsburgh, PA, USA. email: vea1@cdc.gov. Paper number TP-16-002. Original manuscript submitted January 2016. Revised manuscript accepted for publication May 2016. Discussion of this peer-reviewed and approved paper is invited and must be submitted to SME Publications by Feb. 28, 2017.

Introduction

In surface mines, production drilling is an essential process in blasting to fracture the hard rock overburden for removal. During the process, considerable amounts of respirable dust are produced. Past sampling at the shroud area of blasthole drills had documented time-weighted-average respirable dust concentrations ranging from 8.68 to 95.15 mg/m^3 (Organiscak and Page, 1995) and 1.04 to 52.30 mg/m^3 (Listak and Reed, 2007). These high dust concentrations, which may contain silica, can lead to respirable dust overexposures for the miners working nearby. These overexposures can lead to silicosis, an occupational lung disease that has no cure and is ultimately fatal.

Two basic methods are used to control drilling dust: a wet suppression system or a dry collection system (Cecala et al., 2012). Dry drilling techniques using a dust collection system are preferred in rural mining locations where a constant water supply is not available, and in the case of rotary drilling where water is associated with accelerated bit wear due to bearing degradation and hydrogen embrittlement. In addition, dry drilling eliminates freezing-related issues with water in colder climates. Dry dust collectors are highly effective at removing dust, especially the finer material, as long as they are properly operated and maintained (Listak and Reed, 2007; Organiscak and Page, 2005).

In order to understand the respirable dust behaviors around the drill and evaluate the effectiveness of various control techniques, computational fluid dynamic (CFD) simulations can be applied to different scenarios. The focus of this study was on a typical drill deck shroud area of a medium-sized blasthole drill, such as a Sandvik D45KS or Atlas Copco DM45, using a dry dust collection system. The computer model was constructed based upon the existing drill deck/shroud simulator of the

Technical Papers

U.S. National Institute for Occupational Safety and Health (NIOSH). Using information that simulated laboratory test inputs, the CFD model was then validated using two specific data sets from collector-to-bailing airflow ratio experiments conducted in this simulator.

CFD modeling

The ANSYS Fluent Version 15.0 CFD software was used to analyze the airflow and dust distribution in this study. The schematic of the drill table simulator was built according to the geometry measured from the NIOSH full-size facility (Fig. 1) that is fully described in Page, Reed and Listak (2008), Potts and Reed (2008) and Reed and Potts (2010).

To provide airflow in the domain, three major inlet/outlet boundaries were applied (Fig. 1), with no-slip walls with zero heat and diffusive flux as the other boundaries:

- Bailing air inlet: Bailing air with dust is injected into the simulation domain from a circular face inside the hollow drill pipe.
- Roof flow inlet: Fresh airflow is pulled into the simulation domain by the dust collector from the openings in the roof. This intake airflow compensates for the difference of airflow between the dust collector airflow and the bailing airflow.
- Dust collector outlet: Airflow through this outlet is the sum of the bailing and roof airflows. The boundary condition applied is a pressure outlet with 0 Pa (0 psi) gage pressure.

To simplify the CFD model processing, four assumptions are made for the drill shrouds model: (1) the airflow is incompressible, (2) the temperature is constant, (3) the airflow in the domain is fully turbulent and (4) only the leakage at the ground-to-shroud gap is considered.

Both the discrete phase model and species transport model within ANSYS Fluent were evaluated for the drill shroud dust study and compared with the experimental data. In the discrete phase model, dust is treated as a secondary discrete phase (particle) and in the species transport model, dust is considered as a continuous phase (gas). Similar dust distribution patterns can be obtained from both models, but the species transport model is computationally faster, requiring 67 percent less time, and provides smoother concentration results at the sampling points, so it is preferred for modeling dust distribution. Carbon dioxide gas was used to represent dust. The CFD software uses the steady-state Navier-Stokes equations, continuity equations and conservation of energy equations as the basic equations to resolve computer models. Turbulence was modeled using the realizable K-epsilon turbulence model with enhanced wall treatment.

Experimental data and simulation setups. To use CFD to reveal respirable dust behavior, validation assessment is necessary. CFD results have to be authenticated with actual observations to produce valid results. In this study, the CFD model was authenticated with data from a controlled experiment conducted in NIOSH's full-scale drill table simulator.

Table 1 shows the two sets of experimental data used. The bailing airflow was 0.14 m^3/s (300 cfm) in case 1 and 0.24 m^3/s (500 cfm) in case 2. Both cases had laboratory dust concentration data for 2:1, 3:1 and 4:1 collector-to-bailing airflow ratios and a 5.1-cm (2-in.) ground-to-shroud gap (Page and Organiscak, 2004; Page, Reed and Listak, 2008). For each test condition, three or four tests were repeated, and the averaged values were used to calculate the CFD inputs.

The averaged dust feed rate shown in Table 1 cannot be used directly as it is total dust, containing the entire particle size distribution from 0.1 to 300 μm. Only the respirable portion was collected during the experiments, using a 10-mm Dorr-Oliver cyclone and 37-mm filter cassette operated at a flow rate of 2.0 L/min. Therefore, the material was analyzed for its particle size distribution, showing 21.7 percent passing 4.0 μm, which represents respirable dust (Reed, 2011).

Based on the experimental data from Table 1, six simulations were carried out for the bailing airflows of 0.14 m^3/s (300 cfm) and 0.24 m^3/s (500 cfm) and collector-to-bailing airflow ratios of 2:1, 3:1 and 4:1. The values needed for simulation include the bailing airflow velocity, roof airflow velocity, dust collector flow rate and respirable dust mass fraction.

Example of calculation of input parameters. The input parameters for all six simulations were calculated in the same way using the experimental data in Table 1, illustrated here with the case of 0.14 m^3/s (300 cfm) bailing air and 2:1 ratio.

Known values were average bailing airflow = 0.17 m^3/s = 10.39 m^3/min (367 cfm), area of bailing airflow outlet, measured from the laboratory facility = 0.02137 m^2, average collector airflow = 0.33 m^3/s = 20.02 m^3/min (707 cfm), average roof airflow = 0.16 m^3/s = 9.66 m^3/min (341 cfm), area of roof airflow inlet, measured from the laboratory facility = 0.9754 m^2, air density at 25 °C (298.16 K) = 1.184 kg/m^3 and dust mass feed rate = 6.6 g/min.

The bailing airflow velocity and roof airflow velocity were simply calculated based upon quantity equals velocity multiplied by area. The dust concentration needed to be converted to mass fraction of dust in the air, as in the following:

Bailing air mass flow rate
= bailing airflow × air density
= 10.39 m^3/min × 1.184 kg/m^3 = 12.30 kg/min

Figure 1

CFD simulation domain with boundary conditions, samplers' location and cross-sectional planes that display airflow vectors and dust level contours for CFD post-processing.
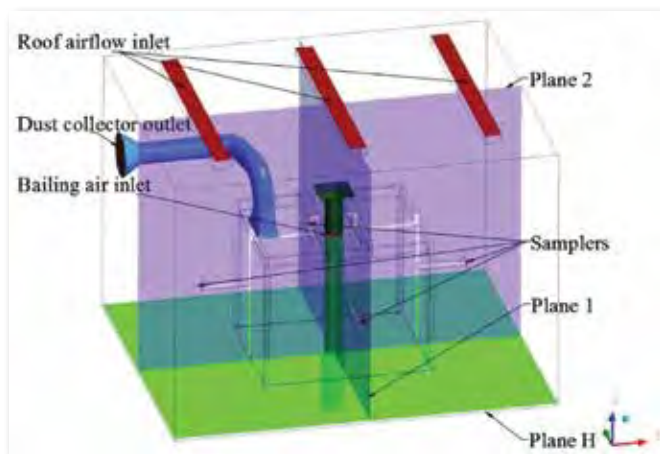
Table 1

Laboratory experimental data with a 5.1-cm (2-in.) ground-to-shroud gap for 0.14 m³/s (300 cfm) and 0.24 m³/s (500 cfm) bailing airflows. Case 1 data are from Page and Organiscak, 2004, and case 2 data from Page, Reed and Listak, 2008.

Case no.	Lab test no.	Bailing airflow (m³/s)	Roof airflow (m³/s)	Collector airflow (m³/s)	Collector-to-bailing air ratio	Dust feed rate (g/min)	Average dust level (mg/m³)
1	B11	0.18	0.17	0.34	1.95	6.4	4.56
1	B15	0.17	0.15	0.33	1.90	6.9	3.81
1	B16	0.17	0.16	0.33	1.92	6.5	3.58
1	**Average**	**0.17**	**0.16**	**0.33**	**1.92**	**6.6**	**3.98**
1	B17	0.17	0.34	0.51	2.97	6.5	0
1	B23	0.17	0.34	0.50	2.97	6.6	1.06
1	B14	0.17	0.34	0.51	2.98	6.6	0.3
1	B30	0.17	0.35	0.52	3.04	6.2	1.5
1	**Average**	**0.17**	**0.34**	**0.51**	**2.99**	**6.5**	**0.72**
1	B19	0.17	0.51	0.69	3.94	6.6	0.02
1	B26	0.17	0.52	0.70	3.97	5.8	0.35
1	B25	0.17	0.53	0.70	4.08	6.6	0.47
1	B31	0.17	0.52	0.69	4.09	6.3	0.36
1	**Average**	**0.17**	**0.52**	**0.70**	**4.02**	**6.3**	**0.3**
2	NB-2	0.24	0.25	0.48	2	5.1	3.3
2	NB-5	0.24	0.23	0.49	1.98	5.2	2.21
2	NB-25	0.24	0.24	0.49	1.98	4.5	1.59
2	**Average**	**0.24**	**0.24**	**0.48**	**1.99**	**4.9**	**2.37**
2	NB-6	0.24	0.48	0.72	3.01	4.8	0.29
2	NB-9	0.24	0.47	0.71	2.98	5.6	0.4
2	NB-12	0.24	0.46	0.70	2.91	4.8	0.88
2	**Average**	**0.24**	**0.47**	**0.71**	**2.97**	**5.1**	**0.52**
2	NB-3	0.24	0.69	0.93	3.88	4.7	0.1
2	NB-13	0.24	0.69	0.93	3.81	4.7	0.11
2	NB-23	0.24	0.71	0.96	3.75	5.1	0.09
2	**Average**	**0.24**	**0.70**	**0.94**	**3.81**	**4.8**	**0.1**

Mass fraction of total dust
= dust mass feed rate / bailing air mass flow rate
= 0.0066 kg/min / 12.30 kg/min = 5.37×10^{-4}
Mass fraction of respirable dust
= mass fraction of total dust × 21.7 percent
= 5.37×10^{-4} × 21.7 percent = 1.17×10^{-4}

Calculating the respirable dust mass fraction to input into the model allows for modeling of respirable dust, but the mass fraction of respirable dust calculated above does not account for the collection efficiency of the sampling cyclone. The Dorr-Oliver cyclone's collection efficiency varies with particle size, following the ACGIH/CEN/ISO curve for sampling efficiency criteria for respirable dust (Gautam and Sreenath, 1997; Gorner et al., 2001; Soderholm, 1989). The curve specifies an approximately 50 percent overall sampling efficiency for particles 4 μm in size, close to 100 percent efficiency for particles smaller than 1 μm, and very low efficiency for particles larger than 10 μm (ACGIH, 1994-1995; Comite Europeen de Normalisation, 1992; International Organization for Standardization, 1995). Therefore, to account for the collection efficiency of the Dorr-Oliver cyclone, the respirable mass fraction must include a correction for cyclone efficiency:

Respirable mass fraction collected
= respirable dust mass fraction × cyclone efficiency
= 1.17×10^{-4} × 50 percent = 5.85×10^{-5}

Technical Papers

Validation by comparing simulations with laboratory experimental results

Table 2 shows the input parameters for the simulations run for the validation study.

The CFD dust concentration used for comparison was the average of the results from the four sampler locations shown in Fig. 1. These CFD concentrations were compared with the averaged experimental dust data from Table 1 at the same locations. Since three or four experimental trials were conducted for each case, each of which produced different dust concentration results, the modeled concentrations were compared with the average experimental concentrations with their 95 percent confidence intervals. If the modeled results were within the experimental 95 percent confidence interval, they were considered acceptable.

Table 3 presents the results showing the comparison. The CFD dust concentrations are within the 95 percent confidence intervals of the laboratory experimental dust concentrations for the 2:1 and 3:1 collector-to-bailing air ratios, validating the model results.

The CFD results for the 4:1 simulation, however, are 0.00 mg/m^3 and not within the 95 percent confidence intervals of the laboratory experimental data. A possible reason for the 4:1 concentrations being higher in the laboratory is dust contamination on the interior facility walls. While the facility was cleaned periodically — approximately weekly — during the series of tests, there was still dust contamination on the interior walls that could result in elevated laboratory dust concentrations. Airflow turbulence within the facility could have re-entrained any wall particles, which is not characterized in the CFD model. This, combined with the fact that both experimental and simulation data showed progressively lower dust levels with increasing ratios, indicates the model may be valid throughout the studied range. Most importantly, the model is valid at a ratio of 2:1, which is typically encountered in the field (Page, Reed and Listak, 2008).

Characteristics of airflow and dust underneath the drill shroud

To portray the shroud airflow velocity vectors and dust concentration contours, cross-sectional plots were developed based upon the orientations of the planes seen in Fig. 1. Two

▆ Table 2

Input parameters for drill shroud dust simulation.

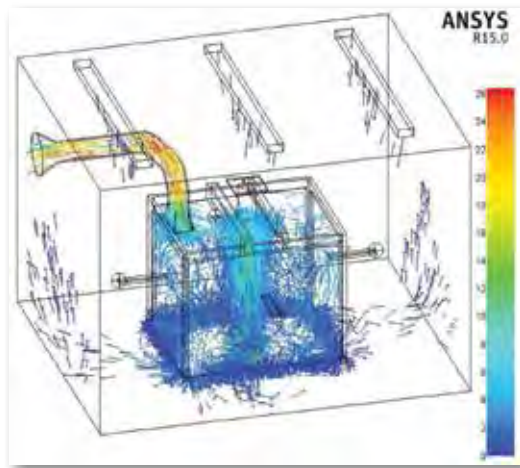| Description	Case 1, 0.14 m³/s (300 cfm) parameters	Case 2, 0.24 m³/s (500 cfm) parameters
Simulation model.	Species transport model.	Species transport model.
Turbulence model.	k-ε, realizable, enhanced wall condition.	k-ε, realizable, enhanced wall condition.
Bailing air inlet (2:1).	Velocity = 8.102 m/s; T = 298.16 K.	Velocity = 11.438 m/s; T = 298.16 K.
Bailing air inlet (2:1).	Dust mass fraction = 5.85 × 10⁻⁵.	Dust mass fraction = 3.07 × 10⁻⁵.
Bailing air inlet (3:1).	Velocity = 8.036 m/s; T = 298.16 K.	Velocity = 11.327 m/s; T = 298.16 K.
Bailing air inlet (3:1).	Dust mass fraction = 5.77 × 10⁻⁵.	Dust mass fraction = 3.22 × 10⁻⁵.
Bailing air inlet (4:1).	Velocity = 8.036 m/s; T = 298.16 K.	Velocity = 11.394 m/s; T = 298.16 K.
Bailing air inlet (4:1).	Dust mass fraction = 5.60 × 10⁻⁵.	Dust mass fraction = 3.02 × 10⁻⁵.
Dust collector outlet (all cases).	Pressure outlet: 0 Pa gage pressure.	Pressure outlet: 0 Pa gage pressure.
Roof flow inlet (2:1).	Velocity = 0.165 m/s, T = 298.16 K.	Velocity = 0.245 m/s, T = 298.16 K.
Roof flow inlet (2:1).	Dust mass fraction = 0.	Dust mass fraction = 0.
Roof flow inlet (3:1).	Velocity = 0.349 m/s, T = 298.16 K.	Velocity = 0.480 m/s, T = 298.16 K.
Roof flow inlet (3:1).	Dust mass fraction = 0.	Dust mass fraction = 0.
Roof flow inlet (4:1).	Velocity = 0.534 m/s, T = 298.16 K.	Velocity = 0.714 m/s, T = 298.16 K.
Roof flow inlet (4:1).	Dust mass fraction = 0.	Dust mass fraction = 0.
Walls.	No-slip boundary conditions and adiabatic walls.	No-slip boundary conditions and adiabatic walls.
Solution method.	Pressure-velocity coupling scheme: coupled; spatial discretization for gradient: Green-Gauss node based; others: 2nd order upwind.	Pressure-velocity coupling scheme: coupled; spatial discretization for gradient: Green-Gauss node based; others: 2nd order upwind.

▆ Table 3

Comparison of the laboratory experimental dust concentrations with 95 percent confidence intervals and the CFD modeled concentrations.

Case 1: 300 cfm	2:1	3:1	4:1
Lab-averaged value, with 95 percent confidence interval (mg/m³).	3.98, 4.56-3.40	0.72, 1.39-0.04	0.30, 0.49-0.11
CFD (mg/m³).	4.07	0.30	0.00
Inside/outside 95 percent CI.	Inside.	Inside.	Outside.
Case 2: 500 cfm	2:1	3:1	4:1
Lab-averaged value, with 95 percent confidence interval (mg/m³).	2.37, 3.35-1.39	0.52, 0.88-0.17	0.10, 0.11-0.09
CFD (mg/m³).	2.46	0.19	0.00
Inside/outside 95 percent CI.	Inside.	Inside.	Outside.

Figure 2

Velocity distribution inside the drill table simulator, for 0.24 m³/s (500 cfm) with 2:1 collector-to-bailing airflow ratio (legend from 0 to 26 m/s).

Figure 3

Velocity vectors for cross-sectional plane H, for 0.24 m³/s (500 cfm) with 2:1 collector-to-bailing airflow ratio (legend from 0 to 26 m/s).

Figure 4

Velocity vectors for cross-sectional plane 1 with a detailed view underneath the table, for 0.24 m³/s (500 cfm) with 2:1 collector-to-bailing airflow ratio (legend from 0 to 26 m/s).

vertical planes, 1 and 2, create cross sections cutting through the shroud. They are perpendicular to each other and to the y- and x-axes, respectively. Each plane has a common line of the drill pipe axis. A third cross-sectional plane, plane H, is a horizontal plane located in the middle of the shroud-to-ground gap, 2.54 cm (1 in.) above the ground surface.

Airflow behavior. Figure 2 shows the the velocity vectors inside the drill table simulator for 0.24 m³/s (500 cfm) airflow. Because the velocity vector plots for 0.14 m³/s (300 cfm) and 0.24 m³/s (500 cfm) were similar, only the 0.24 m³/s (500 cfm) plot is shown. As the bailing air exits the gap between drill stem and drillhole, the upward flow follows along the drill stem to the underside of the table, where it fans out across the bottom of the drill table and continues down the sides of the shroud. This is due to the Coanda effect, under which the airflow tends to attach to nearby surfaces (Trancossi, 2011). This bailing air then strikes the ground, at which point some of it escapes through the gap between the shroud and the ground. This phenomena is illustrated in Figs. 3, 4 and 5.
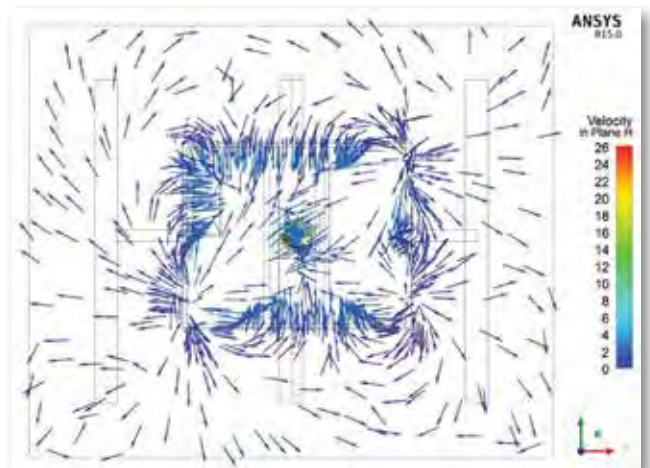
The leakage of airflow from the gap between the shroud and the ground can be clearly observed in the velocity vectors in plane H in Fig. 3. At the three corners without the dust collector inlet, there are flows that leak out of the shroud table, where the velocity vectors are pointing away from the shroud table, providing the potential to emit dust-laden air.

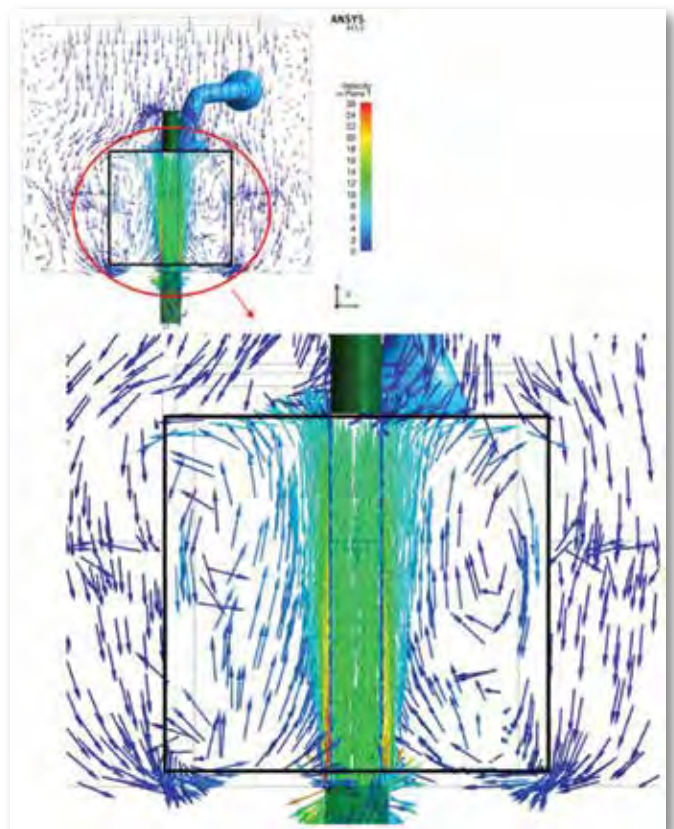Figure 4 shows the velocity vectors for cross-sectional plane 1. This cross section cuts through locations in the shroud-to-ground gap that have strong inward airflows. Due to the forceful inward flow, the downward airflow path is interrupted underneath the table. On the left side inside the drill shroud, the inward airflow blocks the downward flow preventing it from escaping the shroud by redirecting it back into the bailing airflow. The right side displays the same airflow paths inside the drill shroud.

Figure 5 shows the velocity vectors for cross-sectional plane 2. This cross section cuts through locations in the shroud-to-ground gap that do not have strong inward air-

flows. Two areas of circular airflow are created directly underneath the drill table due to the high velocity of bailing airflow. As the downward airflow strikes the ground, part of

the flow continues its circulation back into the bailing airflow with the rest of the flow leaking out of the shroud. The inward airflow at the shroud-to-ground gap from outside the drill shroud is not powerful enough to contain the dust-laden air within the shroud.

As the collector-to-bailing airflow ratio increases from 2:1 to 3:1 and eventually to 4:1, the inward flow from the surrounding outside air through the 5.08-cm (2-in.) shroud-to-ground gap into the shroud table becomes dominant. Minimal, if any, bailing airflow escapes the shroud.

Figure 6 shows the airflow vectors underneath the drill shroud at the 3:1 ratio for cross-sectional plane 2. On the left side beneath the drill table, the collector draws most of the bailing air as it fans out under the table, leaving very little downward airflow. On the right side, the effect of the collector is less. The Coanda effect directs the bailing air down along the inside of the shroud. At the shroud-to-ground gap, it is then diverted toward the drill pipe without escaping the shroud. These strong inward airflow patterns are caused by the increased "makeup airflow" required by the dust collector, resulting in no escaping of this downward airflow. A similar phenomenon is observed for the 4:1 ratio condition.

Respirable dust behavior. From the review of the velocity vectors, there is still airflow escaping the drill shroud at a 2:1 collector-to-bailing airflow ratio, the typical operating condition encountered in the field. This leakage produces a considerable amount of dust from the shroud.

Figure 7 shows the concentration distributions of the respirable dust above 2 mg/m³ for the 0.14 m³/s (300 cfm) case

with 2:1, 3:1 and 4:1 collector-to-bailing airflow ratios. At a 2:1 ratio, the entire space inside the drill shroud simulator is engulfed by the respirable dust. The leakage is greatly reduced at 3:1 and totally confined at 4:1. Similar dust distributions were obtained for the 0.24 m³/s (500 cfm) case with the corresponding collector-to-bailing airflow ratios and are therefore not shown.

Discussion

The CFD simulations show that the shroud structure produces a strong Coanda effect in all three collector-to-bailing airflow ratio conditions. This effect influences the dust-laden bailing airflow such that it attaches to nearby surfaces, follows the route of the drill stem to underneath the drill deck where it fans out and flows down the hanging vertical deck shroud to the shroud-to-ground gap, where the dusty flow strikes the ground and can escape from the gap.

By increasing the collector-to-bailing airflow ratio, the dusty downward airflow is prevented from escaping the shroud when striking the ground. At the ideal condition, the 4:1 collector-to-bailing airflow ratio can effectively prevent almost all dust emissions from the shroud (Fig. 7).

At the 2:1 collector-to-bailing airflow ratio that is typically found in actual drilling operations, considerable amounts of dust leak at various locations in the drill shroud gap, thus reducing the effectiveness of the dust collector. The entire right side of the shroud, where the cab of the drill operator is normally located, has the most intensive dust leakage. This has the potential to adversely affect the working conditions of the drill operator if the cab is opened or not properly sealed.
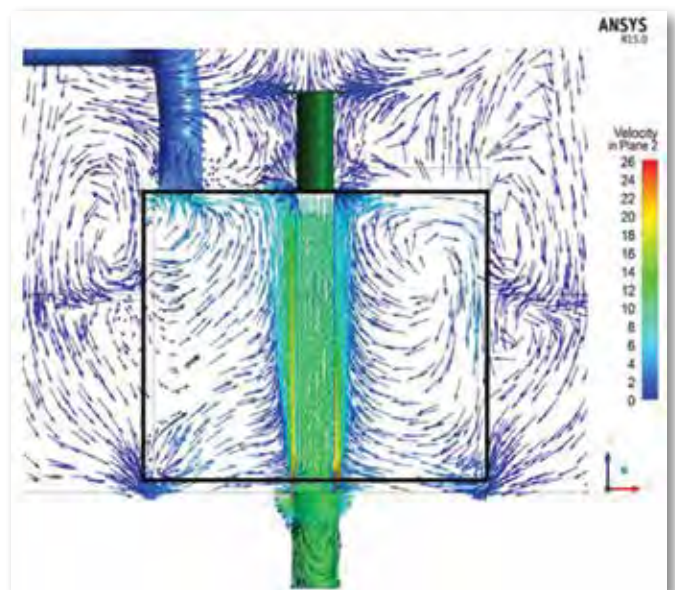
Figure 5

Velocity vectors for cross-sectional plane 2 with a detailed view underneath the table, for 0.24 m³/s (500 cfm) with 2:1 collector-to-bailing airflow ratio (legend from 0 to 26 m/s).
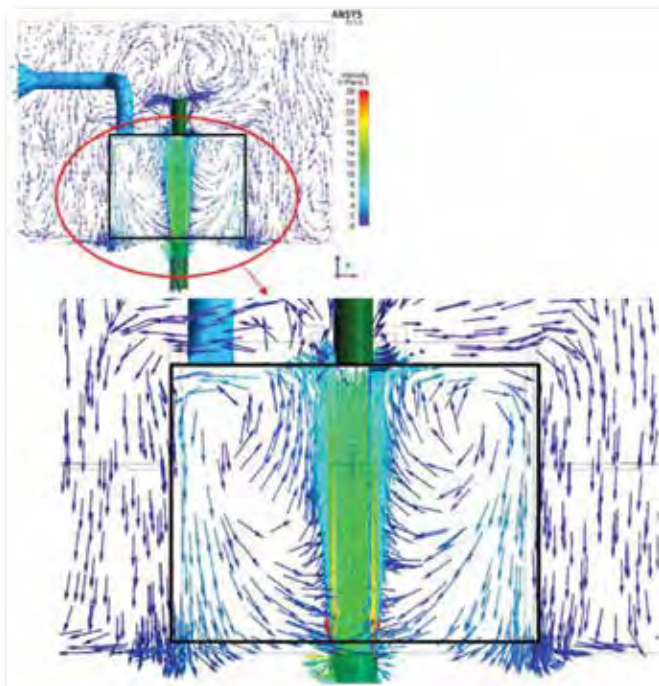
Figure 6

Velocity vectors for cross-sectional plane 2 with a detailed view underneath the drill shroud, for 0.24 m³/s (500 cfm) with 3:1 collector-to-bailing airflow ratio (legend 0 to 26 m/s).

Overall, the escaped dust can affect the surrounding area of the blasthole drill where personnel such as the drill helper and blast crew may be working. With this validated study, future simulations can be performed to help investigate methods to improve dust exposure from drilling operations. ■

Acknowledgments

Disclaimer

References

ACGIH, 1994-95, "1994-1995 Threshold Limit Values for Chemical Substances and Physical Agents and Biological Exposure Indices, Appendix D: Particle Size Selective Sampling Criteria for Airborne Particulate Matter," American Conference of Governmental Industrial Hygienists, Cincinnati, OH.

Cecala, A.B., O'Brien, A.D., Schall, J., Colinet, J.F., Fox, W.R., Franta, R.J., Joy, J., Reed, W.R., Reeser, P.W., Rounds, J.R., and Schultz, M.J., 2012, "Dust Control Handbook for Industrial Minerals Mining and Processing," U.S. Department of Health and Human Services, Centers for Disease Control and Prevention, National Institute for Occupational Safety and Health, DHHS (NIOSH) Publication No. 2012-112, Report of Investigations 9689, 284 pp., http://www.msha.gov/NIOSH/RI9689DustControl.pdf.

Comite Europeen de Normalisation, 1992, "Workplace Atmospheres: Size Fraction Definition for Measurement of Airborne Particles in the Workplace," CEN Standard, EN 481, CEN, Brussels, Belgium.

Gautam, M., and Sreenath, A., 1997, "Performance of a respirable multi-inlet cyclone sampler," Journal of Aerosol Science, Vol. 28, No. 7, pp. 1265-1281, http://dx.doi.org/10.1016/s0021-8502(96)00472-7.

Gorner, P., Wrobel, R., Micka, V., Skoda, V., Denis, J., and Fabries, J., 2001, "Study of fifteen respirable aerosol samplers used in occupational hygiene," Ann. Occup. Hyg., Vol. 45, No. 1, pp. 43-54. http://dx.doi.org/10.1016/s0003-4878(00)00014-4.

International Organization for Standardization, 1995, "Air Quality-Particle Size Fraction Definitions for Health-related Sampling," International Standards ISO Technical Report ISO/TR 7708-1995 (En), ISO, Geneva, Switzerland.

Listak, J.M., and Reed, W.R., 2007, "Water separator shows potential for reducing respirable dust generated on small-diameter rotary blasthole drills," International Journal of Mining, Reclamation, and Environment, Vol. 21, No. 3, pp. 160-172, http://dx.doi.org/10.1080/17480930601176846.

Organiscak, J.A., and Page, S.J., 1995, "Assessment of Airborne Dust Generated from Small Truck-mounted Rock Drills," U.S. Bureau of Mines Report of Investigations 9616, 17 pp, http://www.cdc.gov/niosh/mining/UserFiles/works/pdfs/ri9616.pdf

Organiscak, J.A., and Page, S.J., 2005, "Development of a dust collector inlet hood for enhanced surface mine drill dust capture," International Journal of Mining, Reclamation and Environment, Vol. 19, No. 1, pp. 12-28, http://dx.doi.org/10.1080/13895260412331314248.

Page, S.J., and Organiscak, J.A., 2004, "Semi-empirical model for predicting surface coal mine drill respirable dust emissions," International Journal of Surface Mining, Reclamation, and Environment, Vol. 18, No. 1, pp. 42-59, http://dx.doi.org/10.1076/ijsm.18.1.42.23546.

Page, S.J., Reed, R., and Listak, J.M., 2008, "An expanded model for predicting surface coal mine respirable dust emissions," International Journal of Mining, Reclamation, and Environment, Vol. 22, No. 3, pp. 210-221, http://dx.doi.org/10.1080/17480930701828833.

Potts, J.D., and Reed, W.R., 2008, "Horizontal air-blocking shelf reduces dust leakage from surface drill shroud," Transactions of the Society for Mining, Metallurgy & Exploration, Vol. 324, pp. 55-60.

Reed, W.R., 2011, "Summary of Particle Size Distributions of Typical Drill Cuttings, Dust Collector Material, and Laboratory Test Dust," Internal NIOSH Document, U.S. National Institute for Occupational Safety and Health.

Reed, W.R., and Potts, J.D., 2010, "Improved drill shroud capture of respirable dust utilizing air nozzles underneath the drill deck," Transactions of the Society for Mining, Metallurgy & Exploration, Vol. 326, pp.1-9.

Soderholm, S.C., 1989, "Proposed international conventions for particle size-selective sampling," Ann Occup Hyg, Vol. 33, No. 3, pp. 301-320, http://dx.doi.org/10.1093/annhyg/33.3.301.

Trancossi, M., 2011, "An Overview of Scientific and Technical Literature on Coanda Effect Applied to Nozzles," SAE Technical Paper 2011-01-2591, http://dx.doi.org/10.4271/2011-01-2591.

Figure 7

Respirable dust concentration distributions inside the drill table simulator, for 0.14 m³/s (300 cfm) with 2:1, 3:1 and 4:1 collector-to-bailing airflow ratios (legend from 2 to 40 mg/m³).

collector-to-bailing airflow ratio 2:1

collector-to-bailing airflow ratio 3:1

collector-to-bailing airflow ratio 4:1